Band Structure of the Four Pentacene Polymorphs and Effect on the Hole Mobility at Low Temperature

Alessandro Troisi* and Giorgio Orlandi

Dipartimento di Chimica "G. Ciamician", Universitá di Bologna, via F. Selmi 2, 40126 Bologna, Italy

Received: September 18, 2004; In Final Form: November 24, 2004

The band structure of the four known polymorphs of pentacene is computed from first principles using the accurate molecular orbitals of the isolated molecule as the basis for the calculation of the crystalline orbitals. The computed bands are remarkably different for each polymorph, but their diversity can be easily rationalized using a simple analytical model that employs only three parameters. The effect of the electronic structure on the hole mobility was evaluated using a simple model based on the constant relaxation time approximation. It is found that the mobility tensor is highly anisotropic for three of the four considered polymorphs. The practical implication of this prediction on the technology of thin-film organic transistors is discussed.

Downloaded via ECOLE POLYTECHNIC FED LAUSANNE on March 8, 2022 at 05:50:57 (UTC).
See https://pubs.acs.org/sharingguidelines for options on how to legitimately share published articles.

1. Introduction

The possibility of practical applications for organic semiconductors, demonstrated in the late 1980s[1] and followed by an impressive improvement of the performance and efficiency of the devices based on such materials,[2] have renewed the interest of many researchers toward this field whose first contributions appeared more than fifty years ago.[3] Organic materials (crystals or polymers) based on polyacenes, polythiophenes, and polyetilene have been used to realize light-emitting diodes (LEDs), thin-film transistors (TFTs), and photovoltaic cells, and an increasingly large set of data on these systems are now available.[4−8]

The most important property of these materials is the charge carrier mobility μ, whose lower limit for practical application is 100 $cm^2\ V^{-1}\ s^{-1}$. Organic synthesis provides, in principle, the possibility to fine-tune the charge-transport properties, but the mobility of these materials is very difficult to predict, and the available mobility data lack a proper rationalization. Many groups are therefore active in the development of phenomenological theories[9] and computational models[10−13]to provide reliable predictive and interpretative tools.

In ordered organic materials such as pentacene,[2] the low-temperature transport is described as band-like (i.e., delocalized carriers move coherently across the crystal and are scattered by the lattice phonons). This mechanism is characterized by a power law dependence of the mobility upon the temperature ($\mu \approx T^{-n}$).[14−16] At higher temperatures (∼300 K), polaron transport becomes important; that is, the charge carriers (and their associated lattice deformation) move by thermally activated hopping leading to an Arrhenius-type temperature dependence of the mobility ($\mu \approx \exp(-E_a/kT)$).[17,18] The possibility of a unified description of both transport regimes through suitable effective Hamiltonians is discussed by several authors.[9a,19−21]

While phenomenological theories account qualitatively for the observations, they cannot explain the differences observed for similar materials, for which accurate electronic structure calculations are needed. Analogous materials can show dramatic differences in the transport properties,[22] because the interaction between molecules strongly and subtly depends on structural details. We illustrate this point in the present paper, computing the band structure of the four polymorphs of pentacene and discussing the effect of pentacene polymorphism on the low-temperature hole mobility. Since the first reports of high hole mobility for the pentacene single crystal,[23] several groups studied this[24−28] and related materials[29−31] for their potential application in organic electronics. Several pentacene polymorphs were grown as thin films,[33−38] and one of the thin-film structures was shown to coincide[35] with the bulk single-crystal structure reported by two recent studies.[32,35] A classification and a rationalization was proposed by Mattheus et al.[33] that also found the conditions to reproducibly grow thin films of four crystal forms.[34] The possibility of different transport properties for different growth conditions is of great technological interest. In fact, one of the typical experimental setups involves pentacene thin films, grown on a silicon oxide surface between the source and drain electrodes, forming a prototype of organic thin-film transistors (OTFTs).

To compute the band structure, we propose a first-principles method that uses accurate molecular orbitals computed for the isolated molecule as basis functions for the crystal wave function. A simple analytical model will be proposed to interpret all the band structure, and the results will be further justified through the use of simple orbital overlap arguments. We will not consider in this paper the polaronic mechanism of conduction, limiting our discussion to band-like low-temperature conduction. According to recent measurements,[16] the band-like transport is the dominant one in pentacene up to ca. 300 K.

2. Method

The most commonly used packages[39] for the first-principles computation of band structures have been optimized for the calculation of materials with a relatively small number of atoms in the unit cell and with band gaps ranging from several electronvolts to zero (metals). Molecular crystals contain up to hundreds of atoms per unit cell, and they are usually insulators or semiconductors. The appropriate description of molecular orbitals (MOs) for the isolated molecule requires a split-valence atomic basis set with the inclusion of polarization functions. This basis set makes the calculation of the molecular crystal band structure extremely heavy and the convergence of a self-

10.1021/jp0457489 CCC: $30.25 © 2005 American Chemical Society
Published on Web 01/19/2005

consistent calculation quite problematic. However, in the vast majority of the cases, the electronic coupling between MOs localized on different molecules is much smaller ($\sim$<0.3 eV) than the band gap (>1.5 eV). Under this condition, the localized MOs provide a natural basis for the calculation of the molecular crystal band structure. In the following, we describe the computational method after reviewing, for completeness, the general equations for the calculation of the band structure on a localized basis.

Background. Let $\{\phi_\alpha\}$ be a set of localized one-electron wave functions in an elementary cell (e.g., atomic orbitals or a linear combination of them). The Bloch orbitals (i.e., the basis functions adapted for the translational symmetry) are[39]

$$\psi_\alpha^k = \frac{1}{\sqrt{N}} \sum_T \phi_\alpha(r - T) \exp(ikT) \tag{1}$$

where T is an element of the direct lattice with unit vectors $\vec{a}$, $\vec{b}$, and $\vec{c}$.

$$T = n_a\vec{a} + n_b\vec{b} + n_c\vec{c} \qquad (n_a, n_b, n_c \text{ integers}) \tag{2}$$

and k is a vector of the reciprocal space (unit vectors $\vec{a}^*$, $\vec{b}^*$, and $\vec{c}^*$):

$$k = x_a\vec{a}^* + x_b\vec{b}^* + x_c\vec{c}^* \qquad (x_a, x_b, x_c \text{ real}) \tag{3}$$

The matrix elements of the effective one-electron Hamiltonian are

$$\langle\psi_\alpha^k|H|\psi_\beta^k\rangle = \frac{1}{N}\left\langle \sum_{T'} \phi_\alpha(r - T') \exp(ikT')\middle|H\middle| \sum_T \phi_\beta(r - T) \exp(ikT)\right\rangle \tag{4}$$

$$= \frac{1}{N} \sum_{T'} \sum_T \exp[ik(T-T')]\langle\phi_\alpha(r-T')|H|\phi_\beta(r-T)\rangle \tag{5}$$

The elements in the sum depend on the $T - T'$ difference, and because

$$\sum_{T'} \sum_T f(T - T') = N\sum_T f(T) \tag{6}$$

we get

$$\langle\psi_\alpha^k|H|\psi_\beta^k\rangle = \sum_T \exp(ikT)\langle\phi_\alpha(r)|H|\phi_\beta(r - T)\rangle \tag{7}$$

The relevant matrix elements are conveniently labeled as

$$V_{\alpha\beta T} = \langle\phi_\alpha(r)|H|\phi_\beta(r - T)\rangle \tag{8}$$

In a molecular crystal, the $\{\phi_\alpha\}$ set can be defined by the *molecular orbitals* of the isolated molecule(s) (one set of orbitals for each molecule in the elementary cell). Because the $\{\phi_\alpha\}$ are localized, one can make a (short) list of nonzero $V_{\alpha\beta T}$ elements, which can be determined on a purely geometrical basis.

The Hamiltonian matrix elements are a summation, with a phase factor, over the list of nonzero couplings:

$$H_{\alpha\beta}^k = \langle\psi_\alpha^k|H|\psi_\beta^k\rangle = \sum_T V_{\alpha\beta T} \exp[i2\pi(x_a i + x_b j + x_c k)] \tag{9}$$

where we expressed T and k in terms of their components (eqs 2−3). Because the $\{\phi_\alpha\}$ are non-orthogonal, the overlap matrix elements should be computed as in eqs 8−9:

$$S_{\alpha\beta}^k = \sum_T S_{\alpha\beta T} \exp[i2\pi(x_a i + x_b j + x_c k)] \tag{10}$$

$$S_{\alpha\beta T} = \langle\phi_\alpha(r)|\phi_\beta(r - T)\rangle \tag{11}$$

The band energies for each k value are the solutions of the generalized eigenvalues equation:

$$H^k C^k = S^k C^k \epsilon^k \tag{12}$$

Implementation. For a given crystal structure with m molecules in the elementary cell, the MOs for the different isolated molecules are computed. These orbital energies are the elements $V_{\alpha\alpha(T=0)}$.[40] We used the B3LYP hybrid functional for this computation, but any other method (Hartree−Fock, HF, or density functional theory, DFT) based on the one-electron effective Hamiltonian could be applied. An orbital window around the Fermi energy is selected, because usually few higher-energy occupied orbitals and lower-energy virtual orbitals are sufficient to describe the transport properties (the interaction between selected and excluded orbitals is neglected).

A list of couples of interacting molecules (molecules whose orbitals interact) has been compiled. In our case, we include the interaction between two molecules if the closest distance between their atoms is smaller than a cutoff distance of 5.5 Å. Each couple of molecules is identified by the five-number code: m_1, m_2, [n_a, n_b, n_c]. m_1 and m_2 identify the molecules in the elementary cell; n_a, n_b, n_c identify the translation of the molecule m_2 with respect to m_1. For example, 1 2 [0 0 0] is the coupling between molecules 1 and 2 in the elementary cell, and 1 1 [1 0 0] is the coupling between molecule 1 and its image translated by 1 unit vector a.

The couplings matrix elements $V_{\alpha\beta T}$ and the overlaps $S_{\alpha\beta T}$ are computed between all the considered orbitals on the interacting molecules according to eqs 8 and 11. The Hamiltonian is the same used for the isolated molecule calculation. Because one-electron Hamiltonians depend on the density matrix, one of the greatest difficulties in the calculation of the band structure of metals or small-gap semiconductors is the calculation of the total electron density through integration over the reciprocal space.[39] For a molecular crystal, this step is not necessary, because, to an excellent degree of approximation, the density matrix of the isolated molecule can be used to build the one-electron Hamiltonian for the crystal. Therefore, the electron density is computed self-consistently for the isolated molecule and used to build a tight binding-like Hamiltonian for the crystal.

A grid of points $\{k_i\}$ for which the crystal orbitals have to be computed is selected. For each value k_i, the matrices H^k and S^k are built, and eq 12 is solved for C^k and ϵ^k. The size of the algebraic problem is given by the total number of occupied and virtual orbitals included in the calculation.

Other Tight Binding Schemes. Differently than in other tight binding schemes (EH,[41] DFTB[42]) that compute the tight binding interactions between all the atom pairs, in this approach the strong intramolecular interactions are treated at a high level of accuracy, while the weaker intermolecular interactions are approximated perturbatively. It is therefore possible to arbitrarily improve the description of the MOs by increasing the atomic basis set without increasing the size of the crystal Hamiltonian (eq 12) that always contains the same subset of MOs.

A similar approach was used recently by Cheng et al.[11] that employed a semiempirical Hamiltonian to compute the coupling. An important difference is that we include in this treatment all the couplings between the selected subset of orbitals and not only the coupling between degenerate orbitals. These additional matrix elements could be particularly important in the presence of quasi-degenerate molecular orbitals or in molecular crystals with different molecules in the elementary cell.

Crystal Geometry. We used the unit cell parameters of the four polymorphs as they are listed in Table 2 of ref 33. We also refer to this paper for a description of the crystal structure and a possible explanation for the polymorphism. Here, we identify the polymorphs as **I**, **II**, **III**, and **IV** corresponding to a distance $d(001)$ between their *ab* planes of 14.1, 14.4, 15.0, and 15.4 Å. The experimental determination of their cell parameters is described in ref 35 for polymorph **I** and ref 34 for polymorphs **II**, **III**, and **IV**. Polymorph **I** is the commonly adopted structure in single crystals, and its detailed structure is available from X-ray diffractometry.[35,32] As in other polyacenes, two nonequivalent molecules per unit cell are arranged in herringbone fashion with space group symmetry $P\bar{1}$. The other polymorphs adopt a similar structure, but the detailed crystal geometry was not determined. To make our data set uniform, we performed geometry optimizations of all four polymorphs with the MM3[43] force field, and these geometries were used for the calculations presented in the next section. Many crystal structures of aromatic hydrocarbons were considered in the parametrization of this force field that is therefore expected to also perform well in our case.

To further test the approximation of the method, we also performed geometry optimization *and* band structure calculation using the approximate DFT approach implemented in the code SIESTA.[44] The results, not presented in this paper, indicate that this completely different approach leads to quantitatively similar results for the geometry and the band structure. It is likely that the rigidity of the molecule and the constraints of the unit cell parameters lead to a relatively sharp potential energy minimum that is easily predicted by the various methods.[45]

3. Results and Discussion

Figure 1 shows the results for a band structure calculation of polymorph **I** of pentacene. All ab initio bands are computed using the B3LYP hybrid density functional and the 6-31G(d) basis set. A recent systematic study by Huang and Kertesz[46] shows that this basis set is adequate for the evaluation of the intermolecular coupling and that the error due to the incompleteness of the basis set is <4%. In the calculation, we included HOMO − 1, HOMO, LUMO, and LUMO + 1 for each of the two molecules (eight MOs per unit cell). As expected, the bands appear in couples, each couple originating from the corresponding two quasi-degenerate MOs. The bandwidths are in the range 0.07−0.20 eV, more than one order of magnitude narrower than the ones found in typical inorganic semiconductors.

We are interested in the hole mobility as it can be measured in MOSFET-like devices.[2] In such experiments, a gate electrode injects holes in the material, and these are responsible for the charge transport across the source and drain electrodes. Only the two bands originating from the HOMO orbitals are relevant for the conductance in this case, and we will focus on their description in the following. The structure of the other bands may be of interest, however, for other types of experiments such as photoconductivity measurements[47] or n-type transport in doped semiconductors.[48]

Figure 2 shows the projection of the highest occupied bands along the reciprocal space unit vectors a^*, b^*, and c^* for the four pentacene polymorphs. It is immediately clear that the band structure is very different for the four considered cases. The bandwidth for polymorph **IV** is more than four times larger than for polymorphs **I** and **II**. In the remainder of this paper, we will first show how these large differences can be easily rationalized, and then, we will consider the effect of the computed band structure on the measured hole mobility.

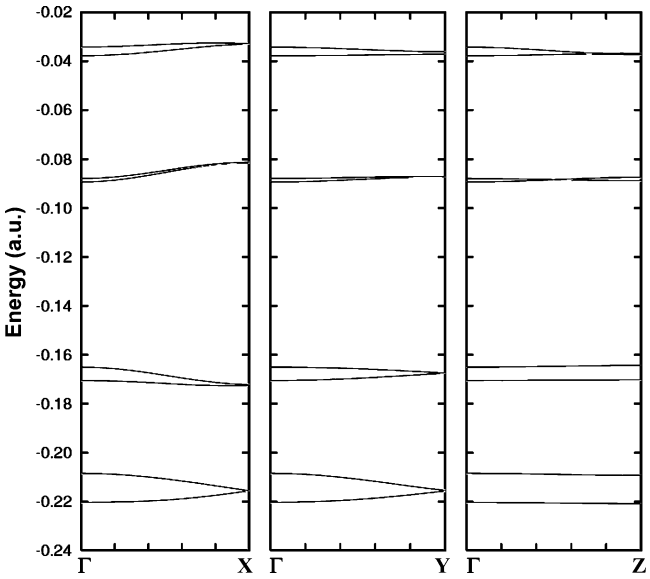

Figure 1. The eight computed bands for polymorph **I** of pentacene (four occupied, four unoccupied). The labeled points indicate the following positions (in terms of reciprocal space unit vectors): Γ (0, 0, 0), *X* ($^1/_2$, 0, 0), *Y* (0, $^1/_2$, 0), *Z* (0, 0, $^1/_2$).

TABLE 1: Couplings (cm^{-1}) between HOMO Orbitals of Close Couples of Pentacene Molecules for the Four Polymorphs[a]

couple of molecules					polymorph				
m_1	m_2	[n_a	n_b	n_c]	**I**	**II**	**III**	**IV**	label
1	1	[0	0	1]	−0.1	0.0	0.0	−0.1	
1	1	[0	1	−1]	−47.8	−60.8	−3.8	−0.5	
1	1	[1	0	0]	411.2	492.6	−232.4	−715.3	A
1	1	[1	1	−1]	−3.2	−3.4	−3.3	8.5	
1	2	[−1	0	1]	0.4	0.1	3.6	3.9	
1	2	[0	−1	1]	−0.2	−0.5	0.0	0.0	
1	2	[0	0	0]	−599.5	−316.5	154.6	805.6	B
1	2	[0	0	1]	−9.8	−9.9	55.6	4.3	
1	2	[0	1	−1]	0.1	0.1	0.0	0.0	
1	2	[0	1	0]	1053.0	970.9	956.9	960.6	C
2	2	[0	1	−1]	−25.8	−41.5	1.3	0.1	
2	2	[1	−1	0]	0.1	0.0	0.0	0.1	
2	2	[1	0	−1]	0.0	0.0	−1.0	−0.1	
2	2	[1	0	0]	400.3	494.2	−320.1	−749.5	A′
2	2	[1	1	−1]	−3.9	−3.7	3.7	−0.5	

[a] Molecular couples equivalent by symmetry are omitted.

Rationalization. Table 1 collects the computed HOMO−HOMO couplings. These are a portion of the couplings included in the calculation, but as we will see, they contain essentially all the needed information. The signs of the couplings are consistent across Table 1 (i.e., the phase of the MO basis is the same for the different polymorphs). It is worth noting that the sign of the intermolecular coupling is important in predicting the overall band structure in two- and three-dimensional crystals, and, therefore, crystal structure calculation purely on the basis of the energy splitting of molecular dimers may lead to incorrect results. The coupling between molecules displaced along the *c* vectors is, as expected, much smaller. Four symmetry-

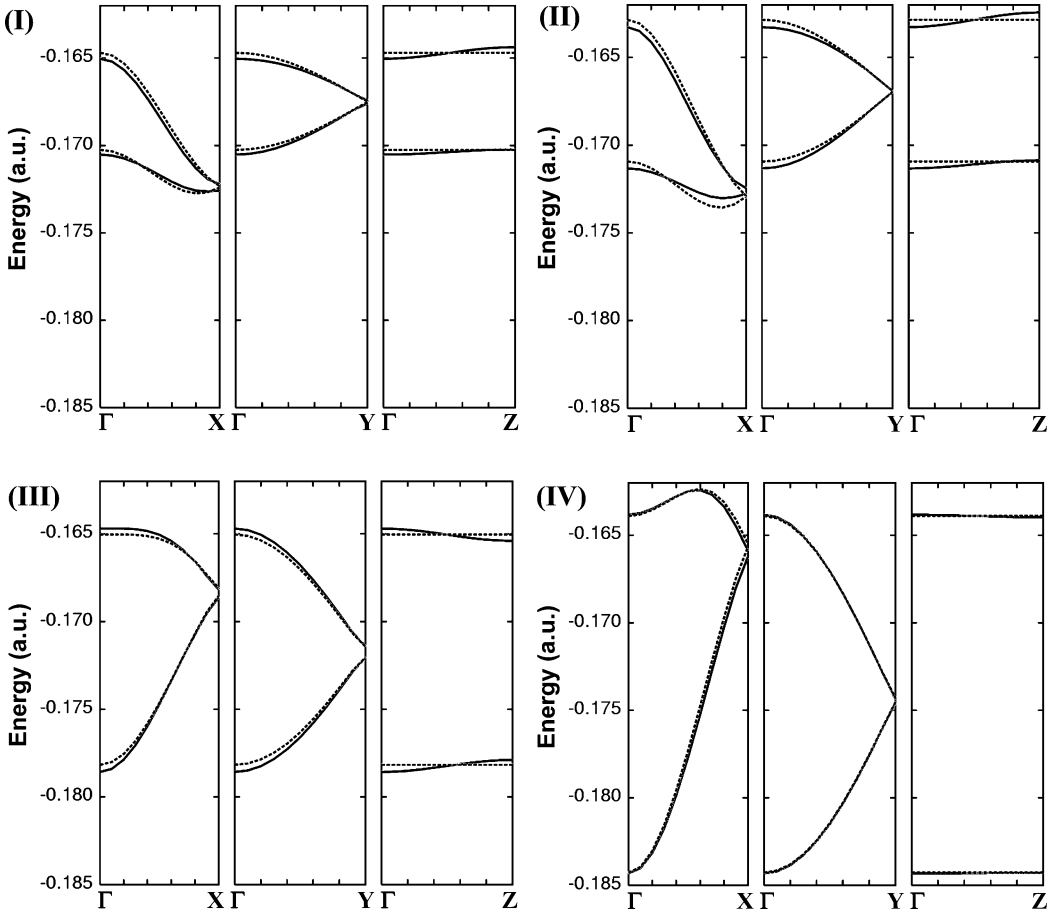

Figure 2. (I−IV) The two highest occupied bands for the four pentacene polymorphs computed as outlined in section 2 (solid lines). Dashed lines show the results of calculations including only the HOMO orbital of each pentacene molecule and only the four major intermolecular couplings. In the approximate calculation, the dispersion along the *c** axis is zero.

independent coupling matrix elements between molecules in the *ab* plane are much larger than the others and determine the structure of the highest occupied bands. We labeled the largest couplings as A, A′, B, and C in Table 1, and we showed the molecules involved in these couplings in Figure 3 (we note that the A and A′ couplings, albeit not identical by symmetry, are very similar in magnitude for the four polymorphs). Figure 2 shows the band structure computed including only the HOMO orbitals, and these four elements are essentially identical to the more accurate calculations using a larger space.

An analytical expression for the higher occupied bands can be derived by taking $A = V_{11[100]} = V_{22[100]}$, $B = V_{12[000]}$, and $C = V_{12[010]}$ and setting to zero the energy of the HOMO orbital on the two molecules. We neglected the intermolecular overlap and used the symmetry relation $V_{\alpha\beta T} = V_{\beta\alpha(-T)}$. Using eq 9, we can write the elements of the 2 × 2 Hamiltonian matrix as

$$H_{11}^k = H_{11}(x_a, x_b) = A\{\exp(i2\pi x_a) + \exp[i2\pi(-x_a)]\} = 2A\cos(2\pi x_a) \quad (13)$$

$$H_{11}^k = H_{22}^k \quad (14)$$

$$H_{12}^k = H_{12}(x_a, x_b) = B[1 + \exp(i2\pi(x_a + x_b))] + C[\exp(i2\pi x_a) + \exp(i2\pi x_b)] \quad (15)$$

The Hamiltonian eigenvalues are

$$E_{1/2}^k = H_{11}(x_a) \pm |H_{12}(x_a, x_b)| \quad (16)$$

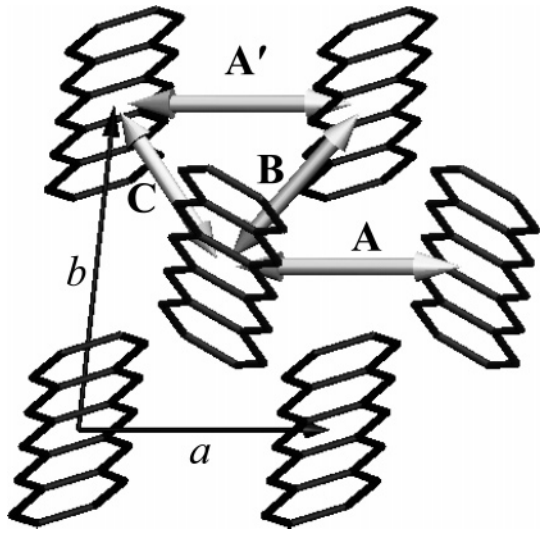

Figure 3. The symmetry-independent couples of molecules (labeled as A, A′, B, C) with the strongest HOMO−HOMO coupling are indicated by the thick arrows. The C coupling is along the *a*−*b* direction: the relative position of the molecules along this direction changes only slightly for the four polymorphs, and consequently, the C coupling is only marginally affected by the polymorphism.

where

$$|H_{12}(x_a, x_b)| = \{2B^2[1 + \cos 2\pi(x_a + x_b)] + 2C^2[1 + \cos 2\pi(x_a - x_b)] + 4BC^2(\cos 2\pi x_a + \cos 2\pi x_b)\}^{1/2} \quad (17)$$

The bands computed using eqs 13−17 are reported in Figure

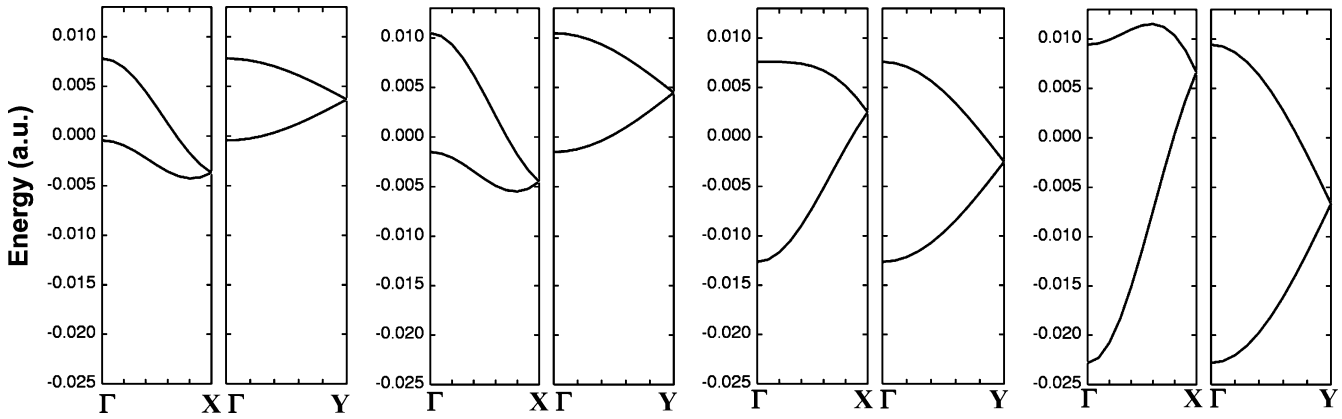

Figure 4. Highest occupied bands computed analytically from eqs 15−17 (to be compared with Figure 2).

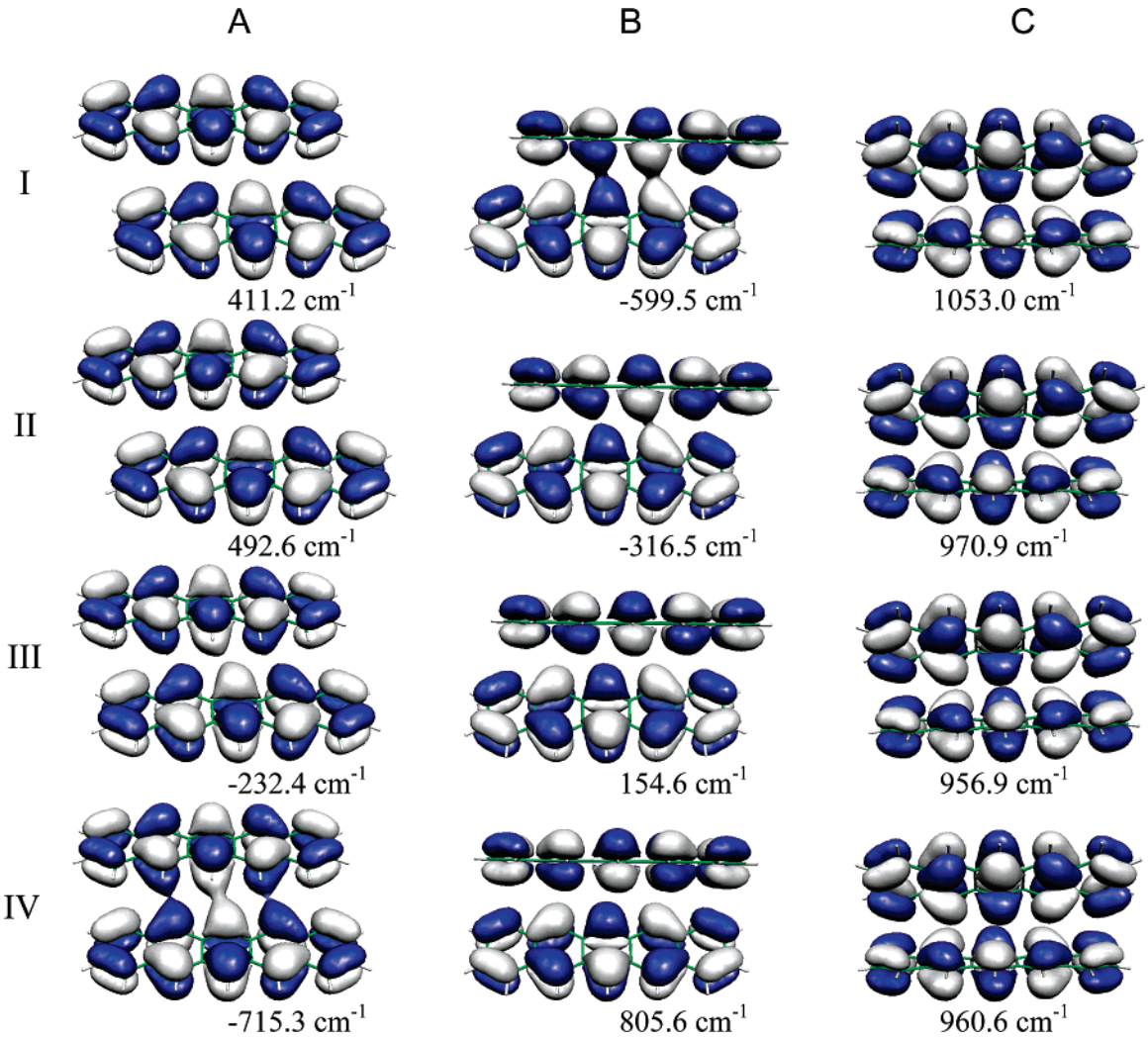

Figure 5. The overlapping couples of orbitals (labeled A, B, C as in Table 1) determining the basic features of the highest occupied bands for the four polymorphs.

4. Interestingly, all the basic features of the complete calculations (Figure 2) are retained using these simple formulas.[49] This suggests that the differences in the highest occupied bands of the four polymorphs can be ascribed almost exclusively to the change in the A, B, and C couplings.

To analyze in detail the relation between the crystal geometry and its electronic structure, we showed in Figure 5 the relative position of the two HOMO orbitals involved in the A, B, C coupling matrix element. As usual, positive overlap corresponds with a negative Hamiltonian matrix element.[51] When going from polymorph **I** to polymorph **IV**, the A and B couplings change sign, while the C coupling is approximately constant. The change in sign is due to a small "sliding" of one molecule with respect to the other that causes the overlap to change from negative to positive in A and from positive to negative in B. This extreme sensitivity of the coupling to apparently minor structural changes was already noticed for other interesting π-stacked systems[50] and is related to the high number of nodal planes in the frontier orbital of conjugated molecules. As also illustrated in Figure 3, the molecules along the $a-b$ axis

maintain their relative position approximately constant in all four polymorphs. For this reason, the polymorphism does not affect the C coupling (that is between molecules along this axis) and influences only the couplings A and B.

We note how this simple rationalization is made possible by the use of the MOs of the isolated molecule as a basis for the calculation and would have not been possible if plane waves or atomic orbitals were used as the basis. The possibility of linking accurate computational results with chemical intuition is particularly important for organic materials whose electrical properties could be, in principle, fine-tuned through chemical synthesis.

Transport Properties. The band-like transport properties of inorganic semiconductors are usually modeled through the semiclassical Boltzmann equation[52] solved using advanced Monte Carlo techniques.[53] This method requires the knowledge of the scattering matrix elements $S_{kk'}$ that express the probability that an electron in the band n and state k is scattered to the state k. Various scattering mechanisms (e.g., crystal defects or lattice thermal vibrations) influence the matrix elements whose calculation from first principles is very demanding. Very often, the scattering matrix elements are taken as parameters and fitted to the experiments.[53−55]

A study of the importance of the different scattering mechanisms was not presented for organic materials such as pentacene, and the absolute mobility is therefore not computable from the band structure alone. However, it is possible to introduce a few approximations that allow a comparison between the transport properties of the different polymorphs.[11] Because the holes in a p-type semiconductor are found almost exclusively in the levels close to the valence band maximum (k^0), the band dispersion can be expanded in a quadratic form around this position:

$$E(k) = E(k^0) - \frac{\hbar^2}{2}\sum_{\mu\nu}(k_\mu - k_\mu^0)(\mathbf{M}^{-1})_{\mu\nu}(k_\nu - k_\nu^0) \quad (18)$$

where μ and ν are one of the Cartesian directions x, y, and z and $\mathbf{M}$ is the inverse of the effective mass tensor:

$$(\mathbf{M}^{-1})_{\mu\nu} = -\frac{1}{\hbar^2}\left(\frac{\partial^2 E(k)}{\partial k_\mu\, \partial k_\nu}\right)_{k^0} \quad (19)$$

We adopt the *relaxation time approximation*,[52] according to which an electron with wave vector k suffers a collision (on the average) every $\tau(k)$ interval, and the state distribution emerging from any collision coincides with the equilibrium distribution.[56] Because all of the collisions occur in a region close to k^0, we also assume a constant (k-independent) relaxation time that leads to the following expression for the mobility:[57]

$$\mu = e\tau\mathbf{M}^{-1} \quad (20)$$

The temperature dependence of the mobility, in our simplified model, is incorporated entirely in the relaxation time τ that is temperature-dependent. When the band-like transport mechanism is the relevant one, the *relative* magnitude of the mobility tensor elements are determined by $\mathbf{M}^{-1}$.

The effective mass can easily be computed from the band structures and provides a straightforward way to compare the effect of the different band structures on the mobility. In Table 2, we reported the inverse effective mass tensor for the four polymorphs together with the position of the valence band maxima. The x axis of the tensor is parallel to the a crystal vector, and the y axis in on the plane defined by the a and b vectors. The isotropic effective mass is not very different for the four polymorphs and is between 2.5 and 3.9 m_e (electronic masses). We note in eq 19 that the effective mass decreases as the band dispersion increases and that it decreases also when the cell dimensions increase (compressing the reciprocal-space dimensions). For this reason, notwithstanding the much smaller dispersion, organic semiconductors based on larger conjugated molecules have an effective mass similar to that of the typical inorganic semiconductors. For a similar reason, the mobility along the c crystal axis (roughly parallel to the z axis) is not much smaller than in the other directions (the c vector being the largest in modulus).[11]

TABLE 2: Results of the Effective Mass Calculation for the Four Polymorphs: Position of the Valence Band Maxima in the Reciprocal Space (expressed as in eq 3), Inverse Effective Mass Tensor (from eq 19), and the Isotropic Effective Mass

		polymorph			
		I	**II**	**III**	**IV**
valence band maximum	x_a	0.377	0.000	0.500	0.706
	x_b	0.465	0.000	0.500	0.958
	x_c	0.988	0.500	0.500	0.725
inverse effective mass tensor (m_e^{-1})	xx	0.058	0.617	0.390	0.406
	xy	−0.092	−0.371	−0.288	−0.091
	xz	0.002	−0.028	−0.018	0.000
	yy	0.504	0.259	0.261	0.316
	yz	−0.041	−0.066	0.005	−0.001
	zz	0.202	0.294	0.269	0.058
average effective mass (m_e)		3.92	2.56	3.26	3.84

Although the τ parameter can be slightly different from polymorph to polymorph (and therefore, the comparison between different polymorphs can be only approximate), a clear difference between the different crystal forms is given by the *anisotropy* of the mobility.[58] This can be better evaluated by computing the principal components of the mobility (i.e., diagonalizing the μ matrix and finding the orthogonal axis that makes μ diagonal).

To simplify our discussion, providing at the same time the most easily verifiable prediction from our model, we considered the two-dimensional conduction through the *ab* plane of the crystal. This is the practically important process in thin-film organic transistors, because the hole migrates between the electrodes driven by a field parallel to the *ab* plane. Moreover, it was suggested that the conduction perpendicular to the *ab* plane is negligible in a real device, because the gate electric field localizes the holes on the interface.[59] We recomputed the bands and the effective mass tensor for the two-dimensional crystal (a monolayer of the (001) plane), and we plotted in Figure 6 the principal components of the mobility tensors (to within a multiplicative constant).

The mobility is extremely anisotropic for polymorphs **I**−**III**, while for polymorph **IV**, it is more uniform in the *ab* plane. This observation is of extreme relevance for the application of pentacene thin layers in an organic transistor. In fact, it is usually not possible to impose the crystal orientation (e.g., the direction of the a axis with respect to the electrodes) in the growth process, while it is possible[35] to control the growth of one particular polymorph. According to our calculation, it is therefore advisable to grow thin layers of polymorph **IV** to build devices with a reduced dependence of the mobility on the orientation.

The largest component of the mobility is directed approximately along the $a-b$ direction, the same direction along

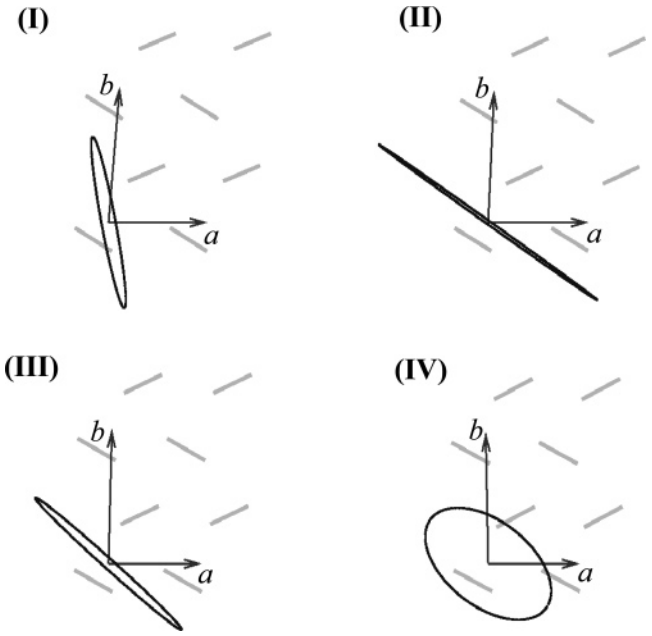

Figure 6. Outline of the (001) plane of the four pentacene polymorphs with the indication of the unit vectors *a* and *b*. The mobility tensor for each case is represented by ellipses: their axes are directed along and proportional to the principal components of the mobility tensor.

which the relative molecular position is constant for all polymorphs. If we compare Figures 5 and 3, it seems that this direction is determined by the strongest intermolecular HOMO−HOMO coupling (labeled as C in Figure 3 and Table 1).[60]

4. Conclusion

In this paper, we computed the band structure of the four known polymorphs of pentacene that can be grown on a silicon oxide substrate. The computed bands are remarkably different for each polymorph. Focusing on the highest occupied band, we showed how these differences can be fully rationalized using a simple analytical expression that depends only on three parameters. This simple analysis is made possible by the use of a molecular orbital basis to express the crystal wave function, a choice that allows a straightforward connection between the numerical results and the chemically intuitive picture of overlapping molecular orbitals. We have found that the largest coupling between the HOMO orbitals involves molecules along the $a-b$ direction, and practically, it stays unchanged from polymorph to polymorph. The other couplings undergo substantial changes that modulate the overall band shape.

A simple method based on the constant relaxation time approximation was used to correlate the computed bands with the hole mobility tensor at low temperature. Studying the hole mobility in the (001) plane, we found that the largest principal component of the mobility tensor is approximately parallel to the $a-b$ direction. The other component is almost negligible for polymorphs **I**−**III**, while it is only slightly lower for polymorph **IV**. A practical consequence of this prediction is that polymorph **IV** should be preferred in an OTFT device whenever the crystal orientation is not controllable to get more reproducible results. Alternatively, one of the other polymorphs can be used provided that the most convenient orientation can be imposed.

Our considerations are limited to the band-like conduction mechanism that applies only at low temperatures. Several quantities computed here (like the intermolecular orbital couplings) can also be used in the analysis of the transport dominated by the small polaron hopping mechanism, and the inclusion of this regime in the modeling is currently under investigation in our group. Another important aspect that needs a careful assessment in the near future is the actual length of the mean free path of the hole (or electron) in organic conductors, a quantity that can be rigorously determined by only including in the model the effects of the electron−phonon coupling.[61] The modeling of transport properties need to be revised if the mean free path of the carriers is close to the device dimension.[62]

Acknowledgment. A.T. wishes to thanks Umberto Ravaioli for helpful suggestions. Work supported by MIUR (projects "Dinamiche Molecolari in Sistemi di Interesse Chimico" and "Microstrutture e nano-strutture a base di carbonio").

References and Notes

(1) Ebisawa, F.; Kurokawa, T.; Nara, S. *J. Appl. Phys*. **1983**, *54*, 3255. (b) Tang, C. W.; Van Slyke, S. A. *Appl. Phys. Lett*. **1987**, *51*, 92. (c) Burroughes, J. H.; Bradley, D. D. C.; Brown, A. R.; Marks, R. N.; Mackay, K.; Friend, R. H.; Burns, P. L.; Holmes, A. B. *Nature* **1990**, *347*, 539.

(2) Dimitrakopoulos, C. D.; Malenfant, P. R. L. *Adv. Mater*. **2002**, *14*, 99.

(3) (a) Eley, D. D. *Nature* **1946**, *126*, 819. (b) Akamatu, H.; Inokutchi, H.; Matsunaga, Y. *Nature* **1954**, *173*, 168.

(4) Pope, M.; Swenberg, C. E.. *Electronic Processes in Organic Crystals and Polymers*; Oxford University Press: Oxford, 1999.

(5) Silinsh, E. A., Čápek, V. *Organic Molecular Crystals: Interaction, Localization, and Transport Phenomena*; AIP: Melville, NY, 1994.

(6) Karl, N. *Synth. Met*. **2003**, 133, 649.

(7) Witte, G.; Wöll, C. *J. Mater. Res*. **2004**, *19*, 1889.

(8) Horowitz, G. *J. Mater. Res*. **2004**, *19*, 1946.

(9) (a) Kenkre, V. M. *Phys. Lett. A* **2002**, *305*, 443. (b) Kenkre, V. M.; Parris, P. E.; *Phys. Rev. B* **2002**, *65*, 245106. (c) Giuggioli, L.; Andersen, J. D.; Kenkre, V. M. *Phys. Rev. B* **2003**, *67*, 045110.

(10) Bredas, J.-L.; Calbert, J. P.; daSilva, D. A.; Cornil, J. *Proc. Natl. Acad. Sci. U.S.A.* **2002**, *99*, 5804.

(11) Cheng, Y. C.; Silbey, R. J.; da Silva Fiho, D. A.; Calbert, J. P.; Cornil, J.; Bredas, J. L. *J. Chem. Phys.* **2003**, *118*, 3764.

(12) Tiago, M. L.; Northup, J. E.; Louie, S. G. *Phys. Rev. B* **2003**, *67*, 115212.

(13) (a) Hutchison, G. R.; Ratner, M. A.; Marks, T. J. *J. Phys. Chem. A* **2002**, *106*, 10596. (b) Hutchison, G. R.; Zhao, Y. J.; Delley, B.; Freeman, A. J.; Ratner, M. A.; Marks, T. J. *Phys. Rev. B* **2003**, *68*, 035204.

(14) Warta, W.; Karl, N. *Phys. Rev. B* **1985**, *32*, 1172.

(15) Karl, N.; Marktanner, J.; Stehle, R.; Warta, W. *Synth. Met.* **1991**, *42*, 2473.

(16) Jurchescu, O. D.; Baas, J.; Palstra, T. T. M. *Appl. Phys. Lett*. **2004**, *84*, 3061.

(17) Nam, M. S.; Ardavan, A.; Cava, R. J.; Chaikin, P. M. *Appl. Phys. Lett*. **2003**, *83*, 4782.

(18) Torsi, L.; Dodabalapur, A.; Rothberg, L. J.; Fung, A. W. P.; Katz, H. E. *Science* **1996**, *272*, 1462.

(19) Fratini, S.; Ciuchi, S. *Phys. Rev. Lett*. **2003**, *91*, 256403.

(20) Ness, H.; Fisher, A. J. *Phys. Rev. Lett*. **1999**, *83*, 452.

(21) Berlin, Y. A.; Burin, A. L.; Ratner, M. A. *Chem. Phys*. **2002**, *275*, 61.

(22) Facchetti, A.; Yoon, M.-H.; Stern, C. L.; Katz, H. E.; Marks, T. J. *Angew. Chem., Int. Ed*. **2003**, *42*, 3900.

(23) (a) Lin, Y. Y.; Gundlach, D. J.; Nelson, S. F.; Jackson, T. N. *IEEE Trans. Electron Devices* **1997**, *44*, 1325. (b) Klauk, H.; Gundlach, D. J.; Nichols, J. A.; Jackson, T. N. *IEEE Trans. Electron Devices* **1999**, *46*, 1258.

(24) Dimitrakopuolos, C. D.; Brown, A. R.; Pomp, A. *J. Appl. Phys*. **1996**, *80*, 2501.

(25) Brown, A. R.; Pomp, A.; de Leeuw, D. M.; Klaassen, D. B. M.; Havinga, E. E.; Herwig, P.; Mullen, K. *J. Appl. Phys.* **1996**, *79*, 2138.

(26) Granstrom, E. L.; Frisbie, C. D. *J. Phys. Chem. B* **1999**, *103*, 8842.

(27) Afzali, A.; Dimitrakopuolos, C. D.; Breen, T. L. *J. Am. Chem. Soc.* **2002**, *124*, 8812.

(28) Zhang, Y. J.; Petta, J. R.; Ambily, S.; Shen, Y. L.; Ralph, D. C.; Malliaras, G. G. *Adv. Mat.* **2003**, *15*, 1632.

(29) (a) Sheraw, C. D.; Jackson, T. N.; Eaton, D. L.; Anthony J. E. *Adv. Mater*. **2003**, *15*, 2009. (b) Payne, M. M.; Delcamp, J. H.; Parkin, S. R.; Anthony. J. E. *Org. Lett.* **2004**, *6*, 1609.

(30) de Boer, R. W. I.; Klapwijk, T. M.; Morpurgo, A. F. *Appl. Phys. Lett*. **2003**, *83*, 4345.

(31) Ito, K.; Suzuki, T.; Sakamoto, Y.; Kubota, D.; Inoue, D.; Sato, F.; Tokito, S. *Angew. Chem., Int. Ed.* **2003**, *42*, 1159.

(32) Holmes, D.; Kumaraswamy, S. Matzeger A.; Vollhardt, K. P. C. *Chem.—Eur. J.* **1999**, *5*, 3399.

(33) Mattheus, C. C.; de Wijs, G. A.; de Groot, R. A.; Palstra, T. T. M. *J. Am. Chem. Soc*. **2003**, *125*, 6323.

(34) Mattheus, C. C.; Dros, A. B.; Baas, J.; Oostergetel, G. T.; Meetsma, A.; de Boer, J. L.; Palstra, T. T. M. *Synth. Met.* **2003**, *138*, 475.

(35) Mattheus, C. C.; Dros, A. B.; Baas, J.; Meetsma, A.; de Boer, J. L.; Palstra, T. T. M. *Acta Crystallogr., Sect. C* **2001**, *C57*, 939.

(36) Fritz, S. E.; Martin, S. M.; Frisbie, C. D.; Ward, M. D.; Toney, M. F. *J. Am. Chem. Soc.* **2004**, *126*, 4084.

(37) Heringdorf, F. J. M. Z.; Reuter, M. C.; Tromp, R. M. *Nature* **2001**, *412*, 517.

(38) Della Valle, R. G.; Venuti, E.; Brillante, A.; Girlando, A. *J. Chem. Phys*. **2003**, *118*, 807.

(39) Pisani, C., Ed. *Quantum-Mechanical Ab Initio Calculation of the Properties of Crystalline Materials, Lecture Notes in Chemistry*; Springer-Verlag: Heidelberg, 1996; Vol. 67.

(40) This approximation is valid for very apolar systems (such as pentacene). In general, the orbital energies need to be corrected for the effect of the crystal field using, for example, an embedding technique.

(41) Haddon, R. C.; Chi, X.; Itkis, M. E.; Anthony, J. E.; Eaton, D. L.; Siegrist, T.; Mattheus, C. C.; Palstra, T. T. M. *J. Phys. Chem. B* **2002**, *106*, 8288.

(42) Margetis, D.; Kaxiras, E.; Elstner, M.; Fauenheim, T.; Manaa, M. R. *J. Chem. Phys.* **2002**, *117*, 788.

(43) (a) Allinger, N. L.; Yuh, Y. H.; Lii, J.-H. *J. Am. Chem. Soc*. **1989**, *111*, 8551. (b) Allinger, N. L.; Li, F.; Yan, L.; Tai, J. C. *J. Comput. Chem*. **1990**, *11*, 868.

(44) Soler, J. M.; Artacho, E.; Gale, J. D.; García, A.; Junquera, J.; Ordejón, P.; Sánchez-Portal, D. *J. Phys.: Condens. Matter* **2002**, *14*, 2745.

(45) Della Valle, R. G.; Venuti, E.; Farina, L.; Brillante, A.; Masino, M.; Girlando, A. *J. Phys. Chem. B* **2004**, *108*, 1822.

(46) Huang, J. S.; Kertesz, M. *Chem. Phys. Lett*. **2004**, *390*, 110.

(47) (a) Tapponnier, A.; Biaggio, I.; Koehler, M.; Gunter, P. *Appl. Phys. Lett.* **2003**, 83, 5473. (b) Peumans, P.; Uchida, S.; Forrest, S. R. *Nature* **2003**, *425*, 158.

(48) Werner, A. G.; Li, F.; Harada, K.; Pfeiffer, M.; Fritz, T.; Leo, K. *Appl. Phys. Lett*. **2003**, *82*, 4495.

(49) The bandwidth obtained from the analytical expression is ca. 1.5 times larger because the intermolecular overlap was neglected. Its inclusion, however, does not lead to a similarly manageable expression.

(50) We have found, as in ref 51, that the Hamiltonian matrix elements are proportional to the corresponding interorbital overlap to an excellent degree of approximation. This observation could be used to develop more approximate treatments.

(51) Troisi, A.; Orlandi, G. *J. Phys. Chem. B* **2002**, *106*, 2093.

(52) Ashcroft, N. W.; Mermin, D. *Solid State Physics*; Holt, Reinhart, and Winston: New York, 1976.

(53) Jacoboni, C.; Reggiani, L. *Rev. Mod. Phys*. **1983**, *55*, 645.

(54) Duncan, A.; Ravaioli, U.; Jakumeit, J. *IEEE Trans. Electron Devices* **1988**, *45*, 867.

(55) Gnani, E.; Reggiani, S.; Rudan, M. *Phys. Rev. B* **2002**, *66*, 195205.

(56) This approximation overestimates the thermalization due to each collision (there is probably a memory of the initial state k), and it neglects the nonequilibrium distribution that is induced when transport properties are measured. On the other hand, these effects are easily captured by interpreting τ as an "effective" time between collisions.

(57) The validity of such an approximation at low temperature was verified in ref 11. Because only the k values close to the band maxima are involved, the most important error introduced by this assumption is due to the direction dependence of τ.

(58) de Wijs, G. A.; Mattheus, C. C.; de Groot, R. A.; Palstra, T. T. M. *Synth. Met.* **2003**, *139*, 109.

(59) Dodabalapur, A.; Torsi, L.; Katz, H. E. *Science* **1995**, *268*, 270; *Appl. Phys. Lett*. **1996**, *68*, 108.

(60) Very similar results (projected in the (001) plane) are obtained when the full 3D crystal is considered.

(61) Coropceanu, V.; Malagoli, M.; da Silva, D. A.; Gruhn, N. E.; Bill, T. G.; Bredas, J.-L. *Phys. Rev. Lett*. **2002**, *89*, 275503.

(62) Datta, S. *Electronic Transport in Mesoscopic Systems*; Cambridge University Press: Cambridge, 1997.